Radio Wave Propagation Characteristics in Lossy Circular Waveguides Such as Tunnels, Mine Shafts, and Boreholes

Christopher L. Holloway, *Member, IEEE*, David A. Hill, *Fellow, IEEE*, Roger A. Dalke, and George A. Hufford, *Life Fellow, IEEE*

***Abstract*—In this paper, we present the characteristics of radio propagation in a circular lossy waveguide whose walls are composed of earth soil materials with frequency-dependent properties. This type of structure is used to represent a radio link for an underground wireless communication channel such as a tunnel, mine shaft, or borehole. We present calculated results of the attenuation constant for various propagation modes in the soil waveguide structure for various soil constituents and moisture levels. Transverse field plots of the various modes for different soil types are also presented. Finally, it is shown that for small $|k_2 a|$ (where k_2 is the wavenumber in the soil and a is the radius of the waveguide) some modes in the waveguide disappear and a discussion of this behavior and how it relates to excitation problems is given.**

***Index Terms*—Circular waveguides, geologic measurement, mining industry.**

I. Introduction

In past years, it was common practice to use a center conductor (i.e., trolley wire) and its ground return as a transverse electromagnetic (TEM) mode communication link in tunnels, mine shafts, and boreholes. Such quasi-TEM mode communication links have been studied extensively by Wait and others [1]–[5]. The use of conductors was advantageous at low frequencies, where waveguide modes are cut off or at least have high attenuation. In some cases additional conductors, such as rails [6] provided a return path, making the tunnel walls less important. However, with the increasing use of wireless communication equipment operating at higher frequencies, there is a need to understand the propagation characteristics of radio waves in tunnels, mine shafts, and boreholes when no wire conductor is present (i.e., a non-TEM mode communication link). This type of propagation environment can be modeled as a circular waveguide with lossy soil walls (Fig. 1).

Electromagnetic wave propagation characteristics of circular waveguides have been studied in detail by many researchers [7]–[23]. However, most of this work has concentrated on either perfectly conducting waveguides or waveguides in which the surrounding medium is lossless (e.g., optical fibers) [19]–[22]. The limited published work on lossy circular waveguides covers only the case for frequency-independent materials over a limited frequency range [12]–[15] and [23].

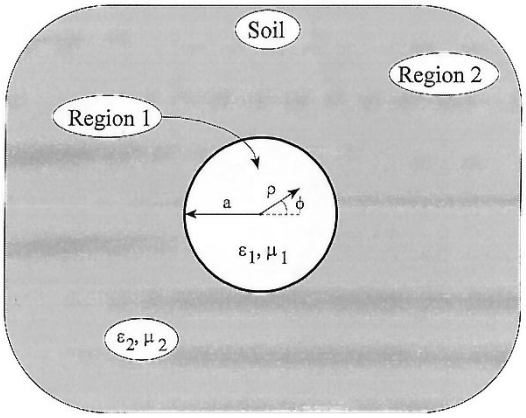

Fig. 1. Cross section of the circular waveguide structure with lossy soil walls.

In this paper, we calculate the attenuation of radio waves over a frequency range of 100 MHz to 10 GHz for a circular waveguide surrounded by a lossy medium with electrical properties characterized by two distinct types of soil with frequency-dependent material properties. This paper is organized as follows. After the introduction, the second section presents mathematical expressions for the electromagnetic fields in the waveguide, along with the transcendental equation that characterizes the modes. The winding number approach is used to solve the complex transcendental equation and this technique is presented in Section III. In Section IV, the calculated attenuation constants for various modes and soil types are presented. Illustrations of the transverse field distribution for different modes are also presented in this section. Finally, we discuss and illustrate that particular modes can disappear for certain frequencies, waveguide dimensions, and soil types.

II. Modal Field Representation

The geometry of the waveguide structure that is used is depicted in Fig. 1. In this analysis, Region 1 is of circular cross section with radius a and has the electrical properties of free-space.

Manuscript received July 27, 1999; revised February 2, 2000.

C. L. Holloway was with the Institute for Telecommunication Sciences, U.S. Department of Commerce, Boulder Laboratories, Boulder, CO 80303 USA. He is now with the National Institute of Standards and Technology, Boulder, CO 80303 USA (e-mail: holloway@its.bldrdoc.gov).

D. A. Hill is with the National Institute of Standards and Technology, Radio Frequency Technology Division, Boulder Laboratories, Boulder, CO 80303 USA.

R. A. Dalke and G. A. Hufford are with the Institute for Telecommunication Sciences, U.S. Department of Commerce, Boulder Laboratories, Boulder, CO 80303 USA.

Publisher Item Identifier S 0018-926X(00)09350-9.

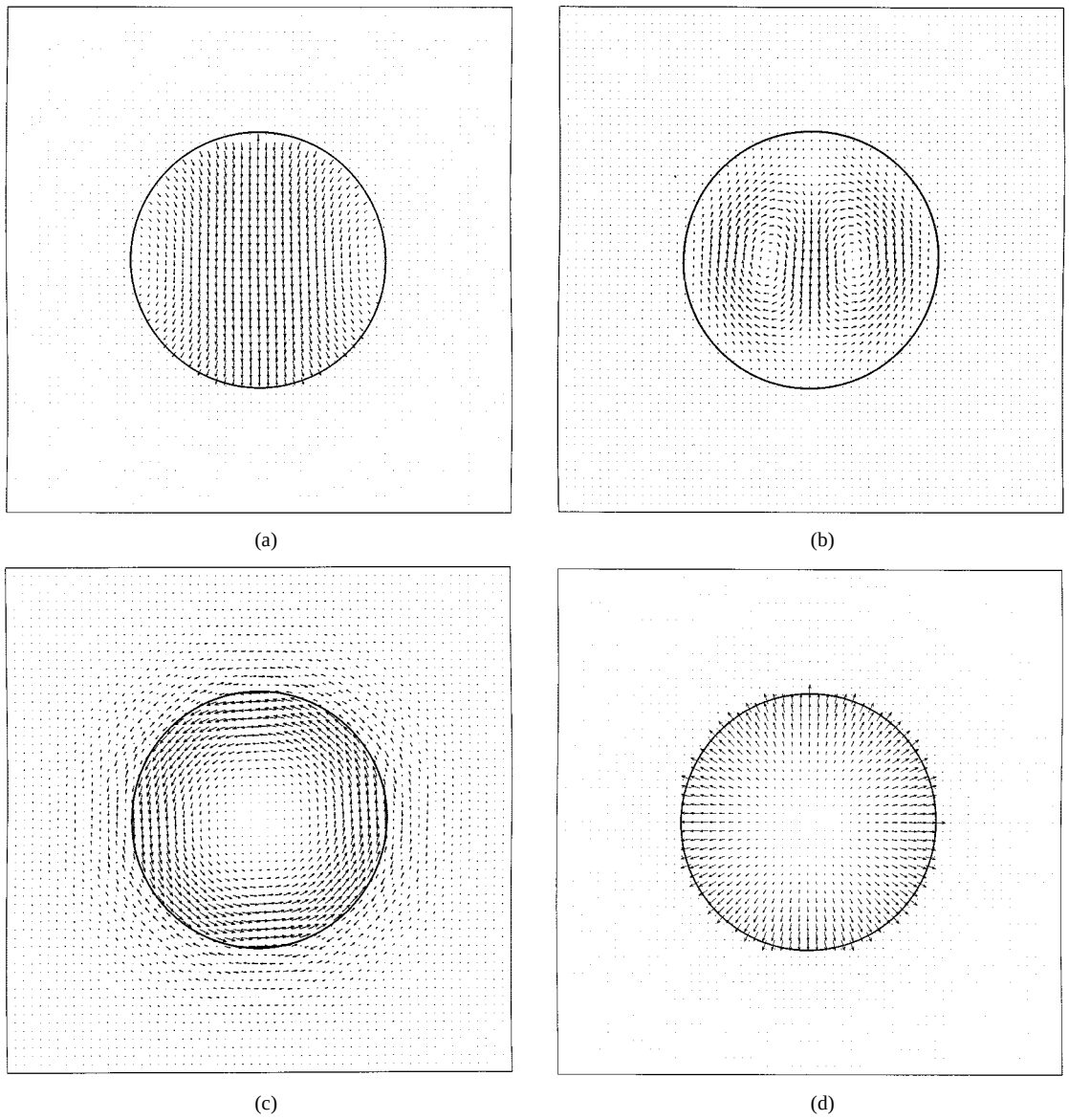

Fig. 2. Transverse electric field distribution for these four types of modes. (a) HE_{11} mode. (b) EH_{11} mode. (c) TE_{01} mode. (d) TM_{01} mode. These results were obtained from Soil I with a moisture level of 25.8% for $a = 38$ cm and at a frequency of 1 GHz.

Region 2 is a lossy medium, characterized by the electrical properties of the various soils under study. A standard cylindrical coordinate system with coordinates denoted by ρ, ϕ, and z is used.

A. Mathematical Form

It can be shown that the ϕ- and ρ-components of the electric (E) and magnetic (H) fields can be obtained from knowing only the z-component of both the E- and H-fields. From Maxwell's equations it can be shown that the z-component of the E- and H-fields must satisfy Helmholtz's wave equation. For this cylindrical geometry, the variables can be separated and the z-components of the fields can be written in the following form:

$$\begin{aligned} E_{z_{1,2}} &= e_{z_{1,2}}(\phi, \rho)e^{-\gamma z} \\ H_{z_{1,2}} &= h_{z_{1,2}}(\phi, \rho)e^{-\gamma z} \end{aligned} \tag{1}$$

where e_z and h_z are functions of ϕ and ρ only and the subscripts 1 and 2 correspond to the fields in regions 1 and 2, respectively. γ is the complex propagation constant of the field and is expressed as

$$\gamma = \alpha + j\beta \tag{2}$$

where α and β are the attenuation and phase constants, respectively.

After substituting (1) into Maxwell's equations and imposing the radiation condition and boundary conditions so that the tangential components of both the E- and H-fields are continuous at a, the z-components of the fields are

$$\begin{aligned} E_{z_1} &= A\cos(\nu\phi)J_\nu(k_1\rho)e^{-\gamma z} && \text{for } \rho < a \\ H_{z_1} &= B\sin(\nu\phi)J_\nu(k_1\rho)e^{-\gamma z} && \text{for } \rho < a \\ E_{z_2} &= C\cos(\nu\phi)H_\nu(k_2\rho)e^{-\gamma z} && \text{for } \rho > a \\ H_{z_2} &= D\sin(\nu\phi)H_\nu(k_2\rho)e^{-\gamma z} && \text{for } \rho > a \end{aligned} \tag{3}$$

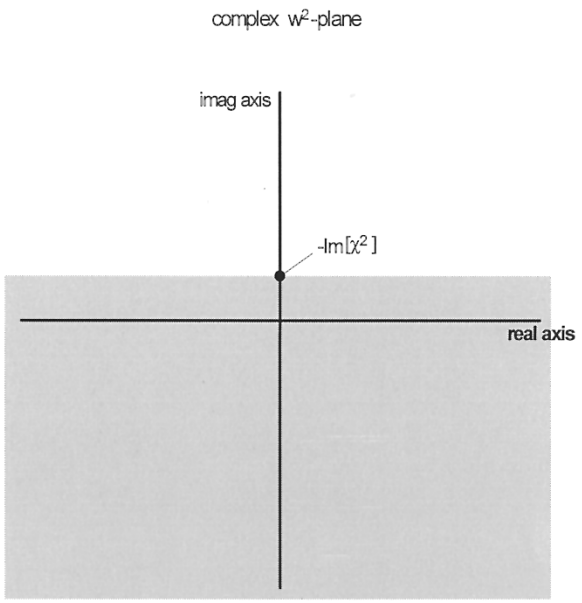

Fig. 3. The complex w^2-plane with the constraint in (21).

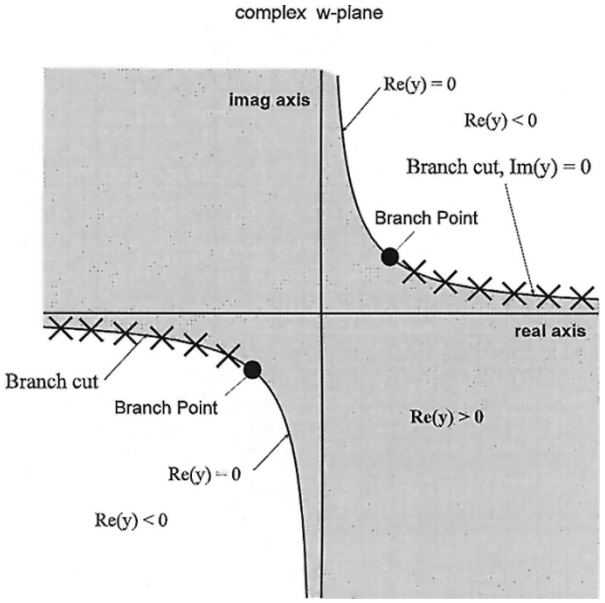

Fig. 4. The complex w-plane: the allowable contour is depicted by the shaded region.

where

$$k_1^2 = \gamma^2 + \omega^2\mu_1\epsilon_1; \quad k_2^2 = \gamma^2 + \omega^2\mu_2\epsilon_2. \tag{4}$$

J_ν represents the Bessel function of the first kind and H_ν represents the Hankel function of the second kind (where the time dependence $e^{j\omega t}$ is assumed). The integer parameter ν is the mode index discussed below, and A, B, C, and D are constants defined as

$$A = 1, \quad B = QH_\nu(k_2a),$$
$$C = \frac{J_\nu(k_1a)}{H_\nu(k_2a)}, \quad D = QJ_\nu(k_1a) \tag{5}$$

and

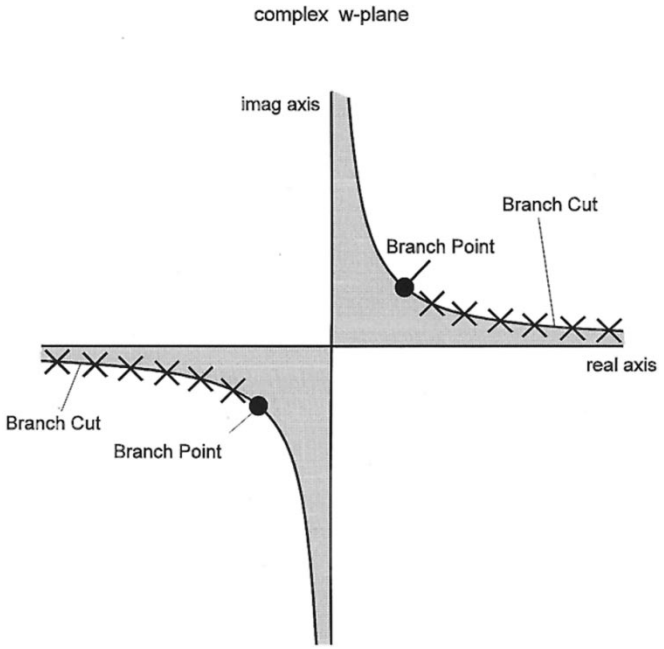

Fig. 5. The allowable contour for searching for the roots of $G(w)$.

$$Q = \frac{\nu\gamma}{a}\frac{1}{j\omega\mu_0}\left[\frac{k_1^2 - k_2^2}{k_1k_2}\right] \cdot \frac{J_\nu(k_1a)}{k_2H_\nu(k_2a)J_\nu'(k_1a) - k_1J_\nu(k_1a)H_\nu'(k_2a)}. \tag{6}$$

As is customary, the primes denote differentiation with respect to the argument. The boundary conditions can also be used to determine the propagation constant γ. In particular, γ for each mode is determined by solving the following transcendental equation of complex order:

$$F_1F_2 = -\left[\frac{1}{w^2} - \frac{1}{y^2}\right]^2(\nu\gamma)^2 \tag{7}$$

where

$$F_1 = \left[\frac{\omega^2\mu_o\epsilon_o}{w}\frac{J_\nu'(w)}{J_\nu(w)} - \frac{\omega^2\mu_2\epsilon_2}{y}\frac{H_\nu'(y)}{H_\nu(y)}\right]$$
$$F_2 = \left[\frac{1}{w}\frac{J_\nu'(w)}{J_\nu(w)} - \frac{1}{y}\frac{H_\nu'(y)}{H_\nu(y)}\right] \tag{8}$$

and

$$w = k_1a; \quad y = k_2a. \tag{9}$$

Using (4), y can be expressed in terms of w and the material properties

$$y^2 = w^2 + a^2\omega^2\mu_o(\epsilon_2 - \epsilon_o) \tag{10}$$

where it is assumed that $\mu_1 = \mu_2 = \mu_o$ and $\epsilon_1 = \epsilon_o$.With y written in this form, the propagation constant is expressed in terms of w

$$\gamma = \sqrt{\left(\frac{w}{a}\right)^2 - \omega^2\mu_o\epsilon_o}. \tag{11}$$

The roots of this expression are the allowed values of the propagation constant γ, which also determines the characteristic

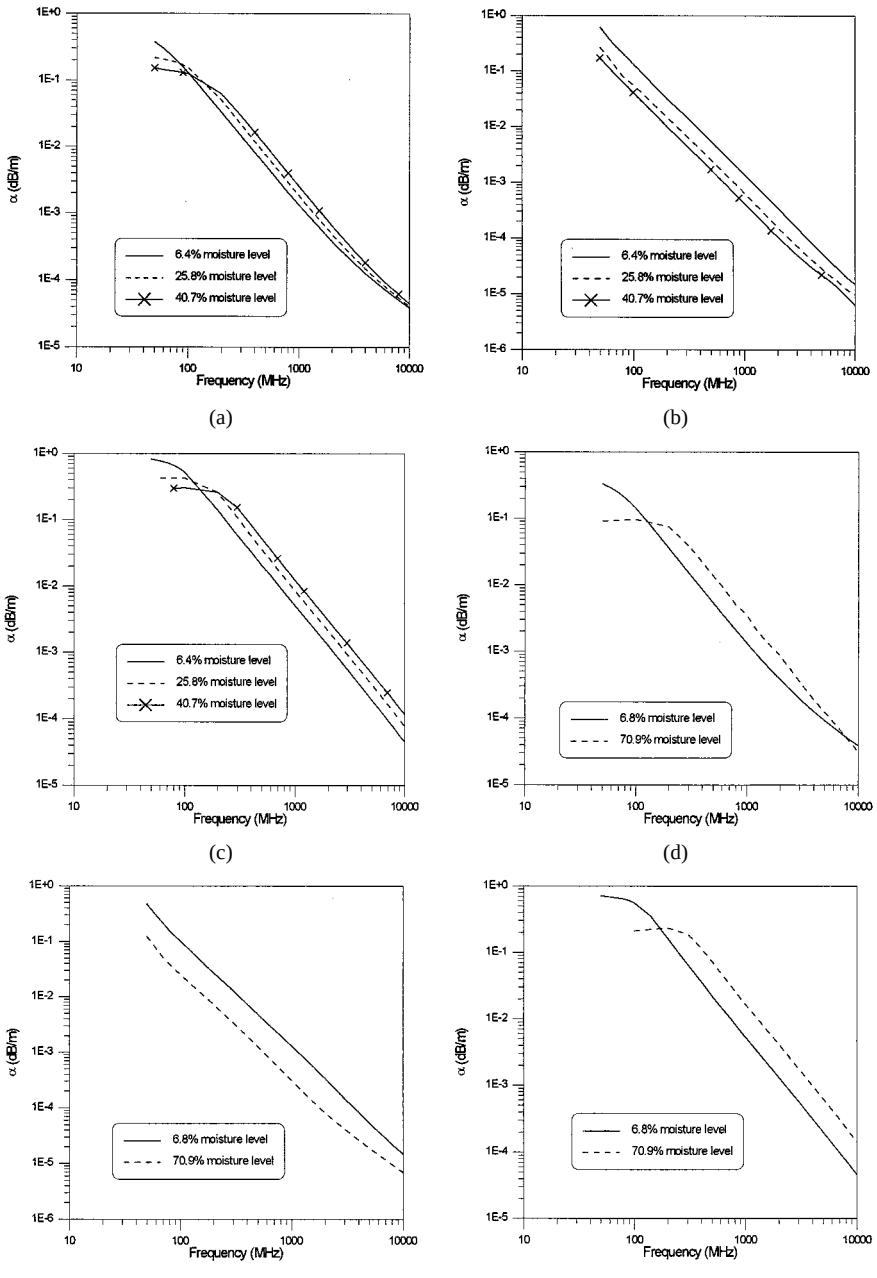

Fig. 6. Attenuation constants for the three dominant modes for a waveguide with a 5 m radius for two types of soil and various moisture levels: (a) HE_{11} for Soil I. (b) TE_{01} for Soil I. (c) TM_{01} for Soil I. (d) HE_{11} for Soil II. (e) TE_{01} for Soil II. (f) TM_{01} for Soil II.

or normal modes of propagation. A discussion of the different modes of propagation is given below.

Once the propagation constant for a particular mode is determined, the z-components of the E- and H-fields can be determined from (3). From Maxwell's equations, the remaining field components can be determined from the z-components of the fields as follows:

$$E_{\phi_{1,2}} = \frac{1}{(k_{1,2})^2}\left[j\omega\mu_o\frac{\partial}{\partial\rho}H_{z_{1,2}} - \frac{\gamma}{\rho}\frac{\partial}{\partial\phi}E_{z_{1,2}}\right]$$

$$H_{\phi_{1,2}} = \frac{1}{(k_{1,2})^2}\left[-j\omega\epsilon_{1,2}\frac{\partial}{\partial\rho}E_{z_{1,2}} - \frac{\gamma}{\rho}\frac{\partial}{\partial\phi}H_{z_{1,2}}\right] \quad (12)$$

and

$$E_{\rho_{1,2}} = \frac{-j\omega\mu_o}{(k_{1,2})^2}\frac{1}{\rho}\frac{\partial}{\partial\phi}H_{z_{1,2}} + \frac{1}{\gamma}\left[\frac{\omega^2\mu_o\epsilon_{1,2}}{\omega^2\mu_o\epsilon_{1,2}+\gamma^2} - 1\right]\frac{\partial}{\partial\rho}E_{z_{1,2}}$$

$$H_{\rho_{1,2}} = \frac{j\omega\epsilon_{1,2}}{(k_{1,2})^2}\frac{1}{\rho}\frac{\partial}{\partial\phi}E_{z_{1,2}} + \frac{1}{\gamma}\left[\frac{\omega^2\mu_o\epsilon_{1,2}}{\omega^2\mu_o\epsilon_{1,2}+\gamma^2} - 1\right]\frac{\partial}{\partial\rho}H_{z_{1,2}} \quad (13)$$

where, as before, the subscripts 1 and 2 correspond to the fields in regions 1 and 2, respectively.

Before we describe methods used to solve the transcendental equation (7), a discussion of the types of modes that can exist in the waveguiding structure is given in the following section.

B. Mode Definitions

The allowable modes are split into four different categories or mode types. The two simplest modes to characterize are the transverse electric (TE_{0m}) and transverse magnetic (TM_{0m}) modes. As usual, the TE modes have no z-component of the E-field; the TM modes have no z-component of the H-field. The subscript "0" indicates that there is no ϕ dependence in the fields and the "m" corresponds to the number of maxima in the field distribution in the ρ direction from $\rho = 0$ to $\rho = a$.

The remaining two mode types are referred to as hybrid modes. That is, there are nonzero E_z- and H_z-field components. These two modes have different designations in the literature. Here, we use the designation given by Snitzer [9], where the hybrid modes are divided into two types depending on the relative contributions of E_z and H_z to the transverse field components. $HE_{\nu m}$ denotes modes where the transverse field component is dominated by the H_z field. For this type of mode, the transverse E field tends to form straight lines. $EH_{\nu m}$ denotes modes where the transverse field component is dominated by the E_z field. For this type of mode, the transverse E field tends to form circular loops. In this nomenclature the subscript "ν" corresponds to the number of times the field changes sign for a rotation in ϕ from 0 to 2π, and the "m" corresponds to the number of maxima in the field distribution in the ρ direction from 0 to a.

Transverse field distributions for these four types of modes for the soil waveguide are shown in Fig. 2. These distributions were obtained from equations (12) and (13). Details of this calculation are given in the following sections.

III. Solving the Transcendental Equation

Unfortunately the transcendental equation (7) that is used to determine the propagation constant cannot be solved in closed form and must be solved numerically. For a numerical solution, we express the roots of the transcendental equation as

$$G(w) = F_1 F_2 + \left[\frac{1}{w^2} - \frac{1}{y^2}\right]^2 (\nu\gamma)^2 = 0. \tag{14}$$

For the TE and TM modes, the transcendental equation reduces to a simpler expression. For $\nu = 0$ the second term of (14) is zero and, hence, either F_1 or F_2 equals zero depending on the type of mode. For the TE_{0m} mode, F_2 must be zero and

$$G(w)_{\mathrm{TE}} = F_2 = 0 \tag{15}$$

and for the TM_{0m} mode, F_1 must be zero and

$$G(w)_{\mathrm{TM}} = F_1 = 0. \tag{16}$$

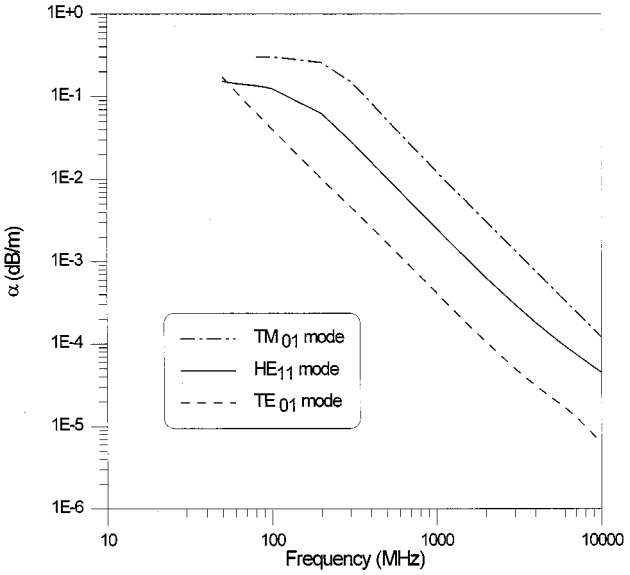

Fig. 7. Comparison between the attenuation constant for the three modes for Soil I with a 40.7% moisture level and a 5 m radius.

A. Possible Solution Methods

There are various methods that can be used to determine the roots (or zeros) of a complex function. Newton's and Müller's methods are common approaches used to determine roots [10]–[15]. Newton's method is easy to implement, however, it does require an initial guess for w. A poor initial guess can result in failure to converge to the root for a particular mode of interest. Approximate methods have also been used to solve (14) (see [14]–[18]), however, these methods have a limited range of validity ($|k_2 a| \gg 1$). In this paper, the so-called "winding number" approach [24]–[26] is used to determine the roots of the transcendental equation. The advantage of this method is that it finds all the roots that lie within a given contour in the complex plane.

B. Winding Number Approach

The winding number of a complex function $G(w)$ is given by [24] and [25]

$$N_o = \frac{1}{j2\pi} \oint_C \frac{G'(w)}{G(w)}\, dw \tag{17}$$

where C is a contour in the complex plane. If the function $G(w)$ has no singularities or branch points within the contour C, then the winding number equals the number of zeros of $G(w)$ inside the contour C. The number of zeros (or the winding number) can also be written as

$$N_o = \frac{1}{2\pi} \arg\left[G(w)\right]\big|_C \tag{18}$$

where $\arg[G(w)]|_C$ denotes the change in the argument of $G(w)$ over the contour C. This expression states that the number of zeros equals the number of times the argument of $G(w)$ winds around some reference axis in the complex plane.

Once the number of zeros within a given contour is known, there are various ways of locating all the zeros within that contour. We have chosen to use the algorithm given by Singaraju *et al.* [26] and modified by Tijhuis and van der Weiden [27].

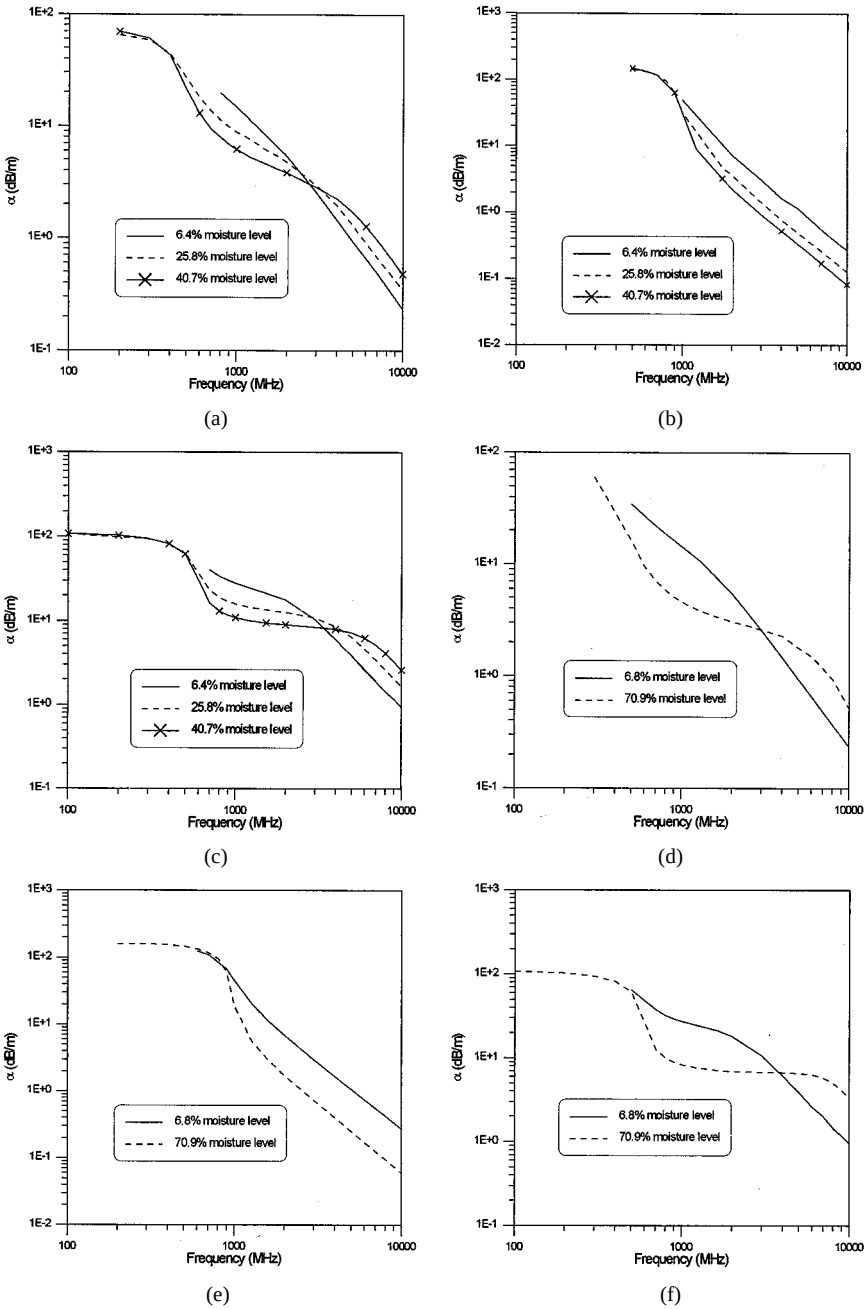

Fig. 8. Attenuation constant for the three dominant modes for a waveguide with a 19 cm radius for two types of soil and various moisture levels: (a) HE_{11} for Soil I. (b) TE_{01} for Soil I. (c) TM_{01} for Soil I. (d) HE_{11} for Soil II. (e) TE_{01} for Soil II. (f) TM_{01} for Soil II.

The winding number approach finds all the roots of an equation that lie within a given contour in the complex plane. The first step in using the winding number approach is to determine a contour within which $G(w)$ is analytic (i.e., a contour free of poles and branch points). Since y and w are related by (10), the branch points of $G(w)$ are given by

$$w_{bp} = \pm j\chi \tag{19}$$

where

$$\chi = \sqrt{a^2\omega^2\mu(\epsilon_2 - \epsilon_0)}. \tag{20}$$

These branch points result from the way y appears (a square root of a quantity involving w) explicitly in $G(w)$ through the $1/y$ term and the Hankel function with argument y.

In order to ensure that waves propagating in the ρ direction in Region 2 (the soil) do not increase exponentially, y must lie in the IVth quadrant in the complex plane. This implies that

$$\mathrm{Im}[w^2] < -\mathrm{Im}[\chi^2] \tag{21}$$

as shown in Fig. 3. Thus, in the w-plane, the allowable contour is bounded by the following hyperbola on which y^2 is pure real

$$\mathrm{Im}[w] = -\frac{1}{2\mathrm{Re}[w]}\,\mathrm{Im}[\chi^2]. \tag{22}$$

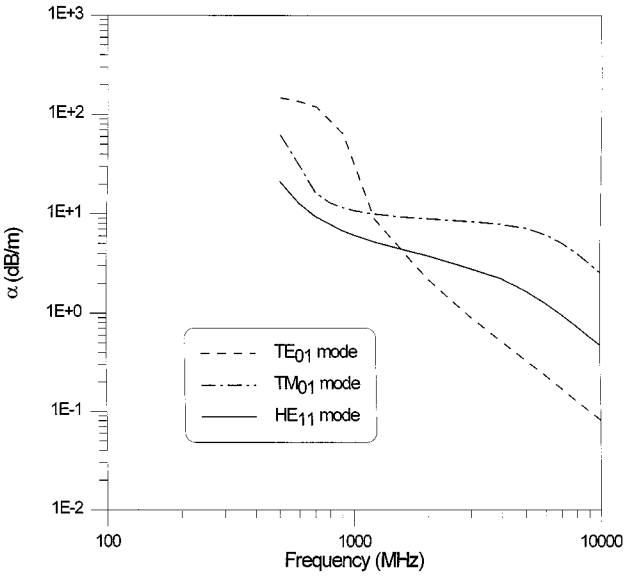

Fig. 9. Comparison between the attenuation constant for the three modes for Soil I with a 40.7% moisture level and a 19 cm radius.

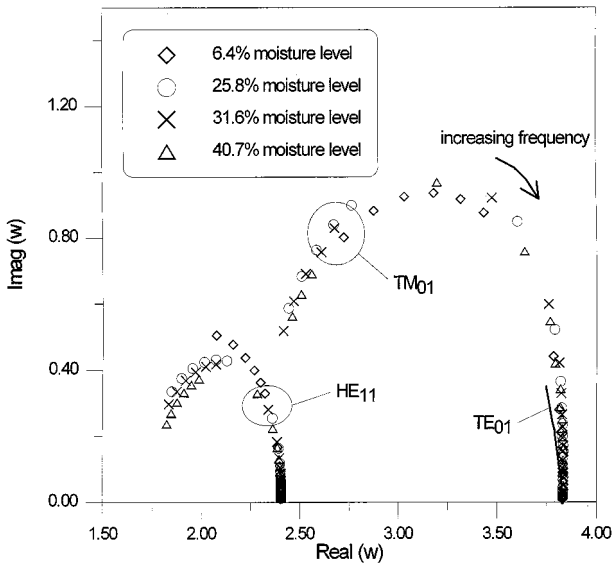

Fig. 10. Location of the roots of the HE_{11}, TM_{01} and TE_{01} modes for Soil I and $a = 5$ m. The root locations of the TE_{01} mode are represented by the solid line (the root locations are essentially identical for the four moisture levels).

The allowable contour is depicted by the shaded region in Fig. 4. The branch cut where $\mathrm{Im}(y) = 0$ runs in only one direction from the branch point where $\mathrm{Re}(y^2) > 0$, as shown in Fig. 3. In the other direction, $\mathrm{Re}(y^2) < 0$ so that y is pure imaginary.

We also want to ensure that the roots of $G(w)$ yield propagation constants that have exponentials of the following form:

$$e^{-\alpha z}e^{-j\beta z} \Rightarrow \text{forward–traveling wave}$$
$$e^{\alpha z}e^{j\beta z} \Rightarrow \text{backward–traveling wave.} \qquad (23)$$

To assure this, the contour must also be bounded by the real and imaginary axes. The allowable contour for searching for the roots of $G(w)$ is depicted by the shaded areas in Fig. 5. The shaded area in the *first* quadrant corresponds to forward-traveling waves, whereas the shaded area in the *third* quadrant corresponds to backward-traveling waves.

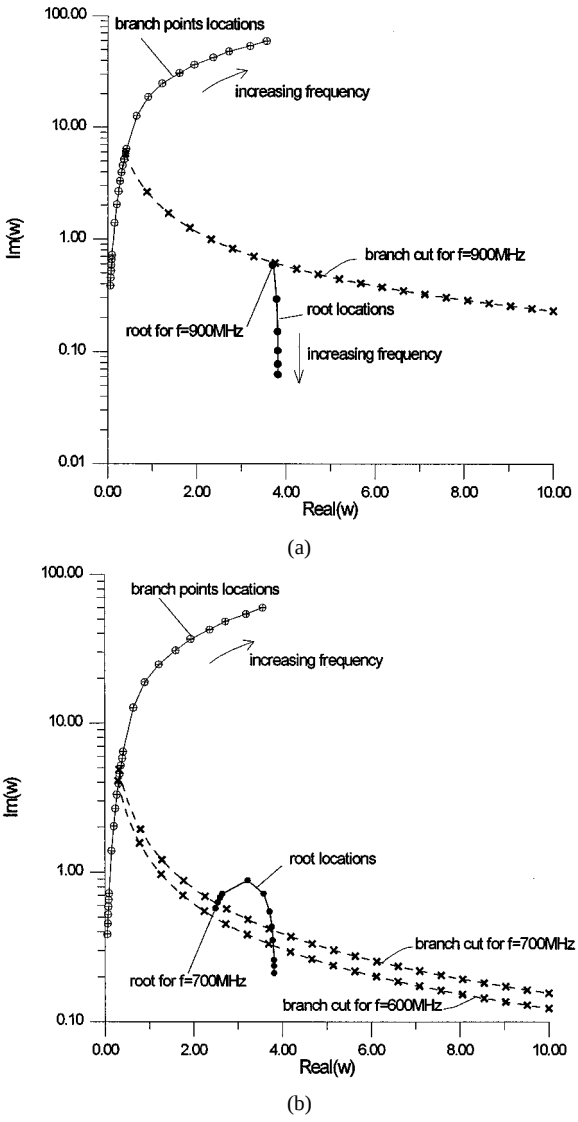

Fig. 11. Illustration of the roots for the TE_{01} and TM_{01} modes approaching the branch cuts for Soil I with a 6% moisture level and $a = 19$ cm. (a) TE_{01} mode. (b) TM_{01} mode.

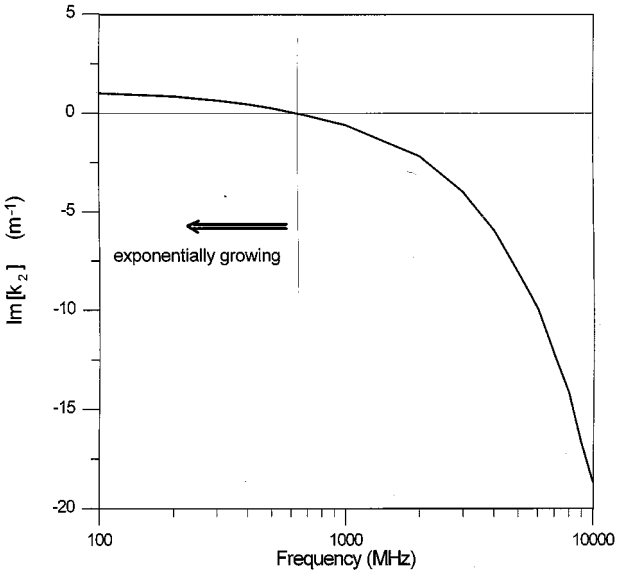

Fig. 12. Propagation constant for a wave propagating along ρ in region 2. The results are for a TM_{01} mode for Soil I with a 6% moisture level and $a = 19$ cm.

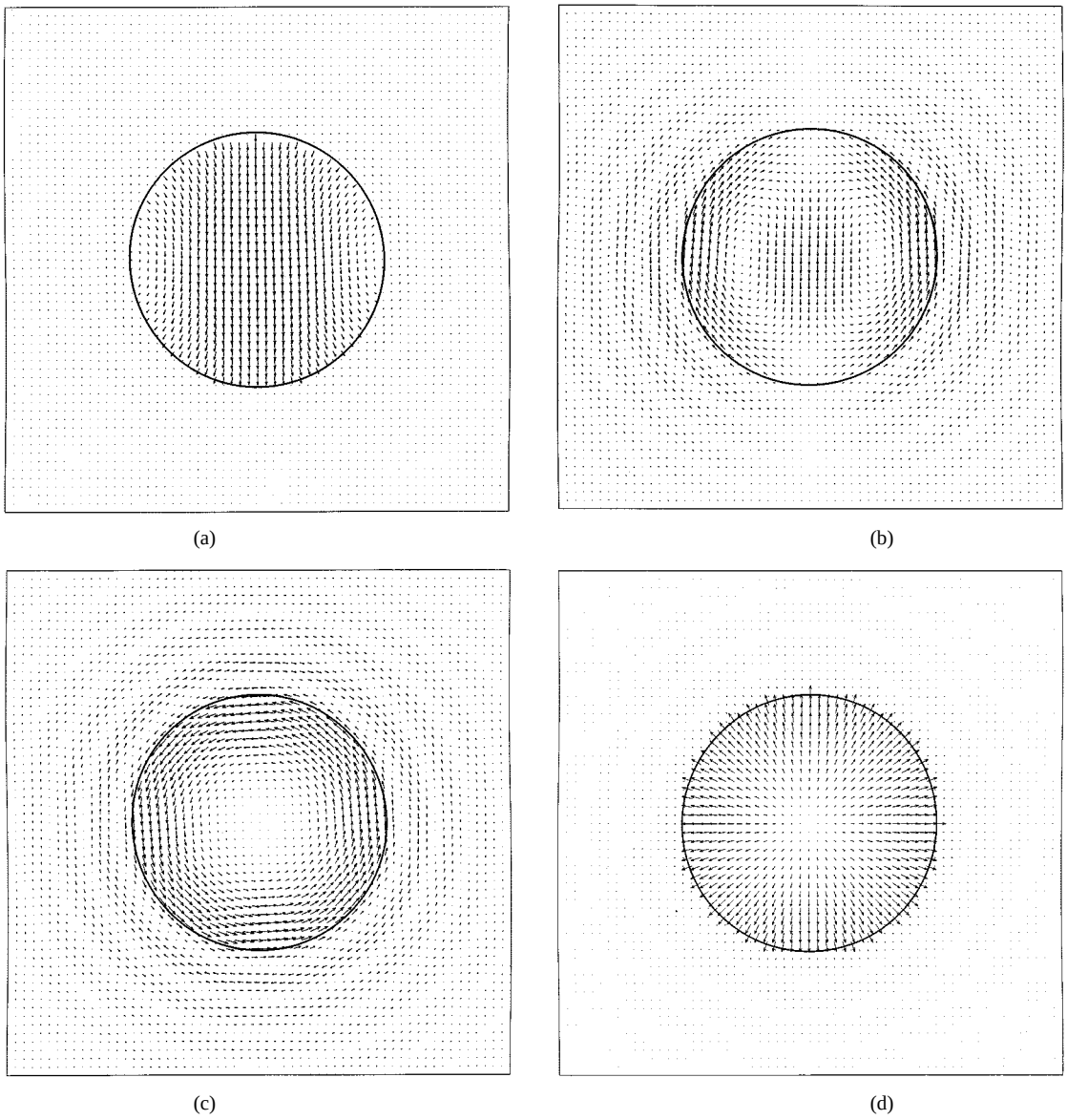

Fig. 13. Transverse electric field distribution for these four types of modes. (a) HE_{11} mode. (b) EH_{11} mode. (c) TE_{01} mode. (d) TM_{01} mode. These results were obtained from Soil I with a moisture level of 25.8% for $a = 38$ cm and at a frequency of 400 MHz.

IV. Numerical Results

A program using the modified winding number algorithm presented by Tijhuis [27] was written to search the shaded area in the *first* quadrant depicted in Fig. 5. In order to avoid the poles of $G(w)$ that occur on the real axis, the bottom of the search area was set just above the real axis ($\mathrm{Im}(w) > 0$). Once the roots of $G(w)$ were determined, the attenuation constant was obtained from the real part of (11). To insure that the root finding procedure was implemented properly, the results were compared to those given in [12]–[14] and [23], with excellent agreement.

Fig. 6 shows results for the three dominant modes for a waveguide with a 5 m radius for two types of soil and various moisture levels. The material properties for the soil are given in the Appendix. Fig. 7 shows a comparison between the attenuation constants for the three modes. Figs. 8 and 9 show results for a waveguide with a 19 cm radius. Notice that the mode type with the smallest attenuation constant changes as the frequency increases. For example, from Fig. 9 it is seen that the HE_{11} mode for $a = 19$ cm has the smallest attenuation up to approximately 1.5 GHz, and above 1.5 GHz, the TE_{01} has the smallest attenuation; while for $a = 5$ m (Fig. 7), the TE_{01} has the smallest attenuation for the entire frequency range of 100 MHz to 10 GHz.

It is interesting to observe the variation of the roots of the transcendental equation for the different modes as a function of frequency. Fig. 10 shows the location of the roots of the HE_{11}, TM_{01}, and TE_{01} modes for Soil I at various moisture levels and frequencies. The root locations for the TE_{01} mode are essentially identical for the four moisture levels. Therefore, to improve clarity of the figure, all the root locations of the TE_{01} mode are represented by the solid line. Notice that the root locations of the TE_{01} mode does not have as much variation across the complex plane (which is confined to the upper frequency locations of the TM_{01} mode) as the other two modes. In general, for increasing frequency, the real parts of the roots for all three modes increases. The real part of the high-frequency roots for the HE_{11} mode approach the real part of the low-frequency

roots for the TM_{01} mode; the high-frequency roots for the TE_{01} mode approach those of the TM_{01} mode. Similar behavior in the location of the roots is also observed in dielectric waveguides with no losses ([11] and [20]).

From Figs. 8 and 9, we see that not all the curves have values down to 100 MHz. For small $|k_2 a|$ the modes approach the branch cut and disappear onto another Riemann sheet. This is illustrated in Fig. 11 for the TE_{01} and TM_{01} modes for a waveguide of $a = 19$ cm. For frequencies below 900 MHz the TE_{01} mode disappears and below 700 MHz the TM_{01} mode disappears. This figure shows that as the frequency decreases, the location of the root approaches the branch cut and eventually goes onto another Riemann sheet. The significance of this in excitation problems is discussed in the next section. This type of behavior, where the mode disappears and enters onto another Riemann sheet, is also found in other types of waveguiding structures [28]–[30].

If the search is continued on the other side of the branch cut, roots will be found. However, these roots will result in exponentially growing waves. This is illustrated in Fig. 12, which presents the propagation constant for a wave propagating radially (along ρ) obtained from the root of $G(w)$ as the branch cut is crossed. Below about 700 MHz, the imaginary part of k_2 obtained from the root is positive and, hence, the wave grows exponentially. Similar results for a surface wave in an absorbing layer are given in [30].

Once the propagation constants are determined, the transverse field for various modes can be obtained. Figs. 2 and 13 illustrate the transverse field distributions for the HE_{11}, EH_{11}, TM_{01}, and TE_{01} modes, for frequencies of 1 GHz and 400 MHz, respectively. As expected, the lower-frequency signals penetrate farther into the soil. The field distributions for the TE_{01}, TM_{01}, HE_{11}, and EH_{11} modes of the lossy (i.e., soil) waveguide are similar to the field distributions for the TE_{01}, TM_{01}, TE_{11}, and TE_{12} modes of a perfectly conducting waveguide, respectively. One distinguishing feature of the TE_{01} mode for the soil waveguide as compared to the TE_{01} mode for the perfectly conducting waveguide is that the tangential E fields at $\rho = a$ in the soil are not zero (as with a perfectly conducting guide).

From Fig. 13, it appears that there is very little field penetrating into the lossy soil for the HE_{11} and the TM_{01} modes, while the EH_{11} and TE_{01} modes clearly penetrate the lossy soil and then exhibit very rapid amplitude oscillation as a function of ρ once in the lossy soil. Actually all four modes penetrate the lossy soil and exhibit this very rapid field variation. This variation is masked in the vector field plots for the HE_{11} and TM_{01} mode since the amplitude of the fields in the air region are significantly larger than the fields in the soil for these two modes. This is explicitly illustrated in Fig. 14, where the normalized field amplitudes for the HE_{11} and TE_{01} modes in the two regions are depicted. This figure shows that there is an order of magnitude difference in the field in the two regions for HE_{11} mode, while for the TE_{01} mode the field differs by only a factor of two.

Additional soil types with frequency dependent properties are given in [33]. Waveguides with these additional soil types were analyzed and results similar to those presented here were obtained.

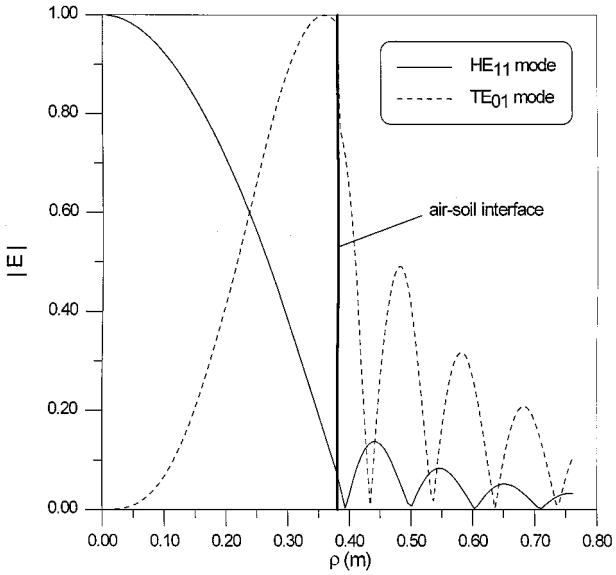

Fig. 14. Normalized amplitude of fields in the two regions for the HE_{11} and TE_{01} modes. These results were obtained from Soil I with a moisture level of 25.8% for $a = 38$ cm and at a frequency of 400 MHz.

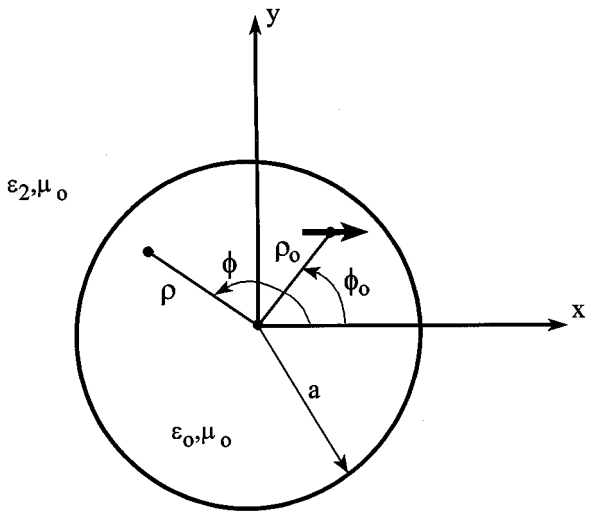

Fig. 15. Geometry for an x-directed electric dipole source in a circular waveguide.

V. Excitation of Modes

The excitation problem is important both for practical transmission applications [34] and for illustration of the relative importance of the discrete waveguide modes and the continuous spectrum. We chose a transverse Hertzian dipole source because it avoids the need to solve for the current distribution and because it can excite all the modes. The geometry for an x-directed electric dipole of moment Ids located at $(\rho_o, \phi_o, 0)$ is shown in Fig. 15.

The solution for the fields of this problem has been given previously with application to determining the change in the dipole impedance due to the waveguide walls [35]. The secondary fields (due to the waveguide walls) can be derived in terms of the z components of the fields, which are given in [35] in terms of modified Bessel functions [36]. If we convert those

results to our notation, the z components of the secondary fields in the waveguide ($\rho < a$) are

$$\left.\begin{matrix} E^s_{z_1} \\ H^s_{z_1} \end{matrix}\right\} = \sum_{\nu=-\infty}^{\infty} \int_{-\infty}^{\infty} \left\{\begin{matrix} P_\nu(k_z) \\ Q_\nu(k_z) \end{matrix}\right\} \cdot k_1^2 (-j)^\nu J_\nu(k_1\rho) e^{-j[\nu(\phi-\phi_o)+k_z z]}\, dk_z \quad (24)$$

where k_1 is defined above. The propagation constant γ and the axial wavenumber k_z are related by $\gamma = jk_z$. The ν summation is taken over all integers, and the k_z integration is taken along the real k_z axis. The precise forms of the coefficients, P_v and Q_v, are not needed for this discussion, but are given in [35]. For other sources, the general form of (24) would hold, but the coefficients would change.

In the dipole impedance application [35], the k_z integrations were evaluated at $z = 0$ by numerical integration along the real axis. To illustrate mode excitation, we need to deform the integration path in the complex k_z plane. We start by rewriting the coefficients in a form that displays their poles explicitly

$$\left.\begin{matrix} P_\nu(k_z) \\ Q_\nu(k_z) \end{matrix}\right\} = \frac{1}{D_\nu(k_z)} \left\{\begin{matrix} R_\nu(k_z) \\ S_\nu(k_z) \end{matrix}\right. \quad (25)$$

where $D_\nu(k_z) = G(w)$ and $G(w)$ is defined in (14). Thus, the poles of the coefficients determined from $D_\nu = 0$ are the same as the zeros of $G(w)$ and R_ν and S_ν have no poles.

In addition to poles, the integrand also has branch cuts in the k_z plane. From (4), we see that there are branch points at $k_z = \pm\sqrt{\omega^2\mu_o\epsilon_2}$. As with the previous w-plane analysis, we need to establish branch cuts so that $\mathrm{Im}(k_2)$ is negative throughout the k_z plane. The branch cuts where $\mathrm{Im}(k_2) = 0$ are determined by the hyperbola

$$\mathrm{Im}(k_z) = \frac{\mathrm{Im}(\omega^2\mu_o\epsilon_2)}{2\mathrm{Re}(k_z)} \quad (26)$$

along with the second condition

$$\mathrm{Re}^2(k_z) - \mathrm{Im}^2(k_z) < \mathrm{Re}(\omega^2\mu_o\epsilon_2) \quad (27)$$

which is required so that k_2 is real on the branch cuts. Equation (27) determines that the branch cuts run from the branch points toward the imaginary axis, as shown in Fig. 16.

For positive z, we can deform the integration contour from the real axis into the negative k_z half plane so that we pick up the pole residue series and the branch-cut integral, as shown in Fig. 16. (For negative z, we would make the analogous deformation into the positive k_z half plane.) The contribution from the semicircle at infinity vanishes because of exponential attenuation. So we can rewrite (24) in the following form:

$$\left.\begin{matrix} E^s_{z_1} \\ H^s_{z_1} \end{matrix}\right\} = \sum_{\nu=-\infty}^{\infty} (-j)^\nu e^{-j\nu(\phi-\phi_o)} \cdot \left[\int_{\text{branch}} \left\{\begin{matrix} P_\nu(k_z) \\ Q_\nu(k_z) \end{matrix}\right\} k_1^2 J_\nu(k_1\rho) e^{-jk_z z}\, dk_z - j2\pi \sum_m \left\{\begin{matrix} R_\nu(k_{z\nu m}) \\ S_\nu(k_{z\nu m}) \end{matrix}\right\} \cdot \frac{k_{z\nu m}^2 J_\nu(k_{1\nu m}\rho)}{D'_\nu(k_{z\nu m})} e^{-jk_{z\nu m}z}\right] \quad (28)$$

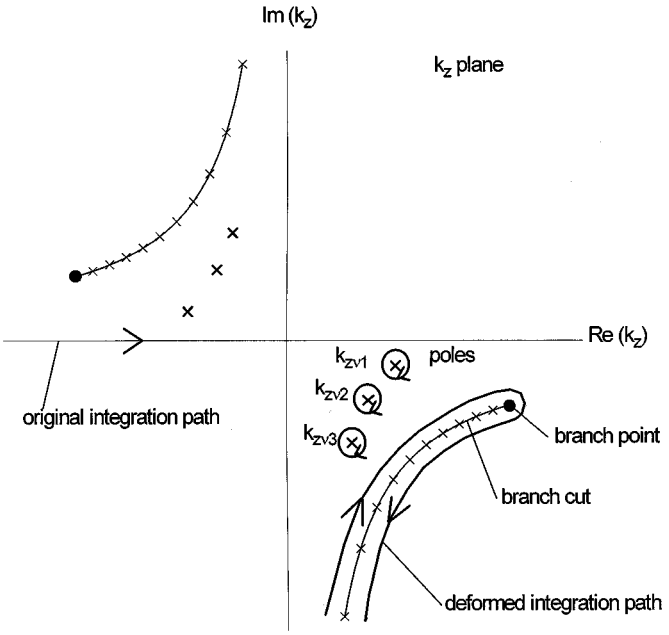

Fig. 16. Pole locations, branch cuts, and integration contours in the k_z plane.

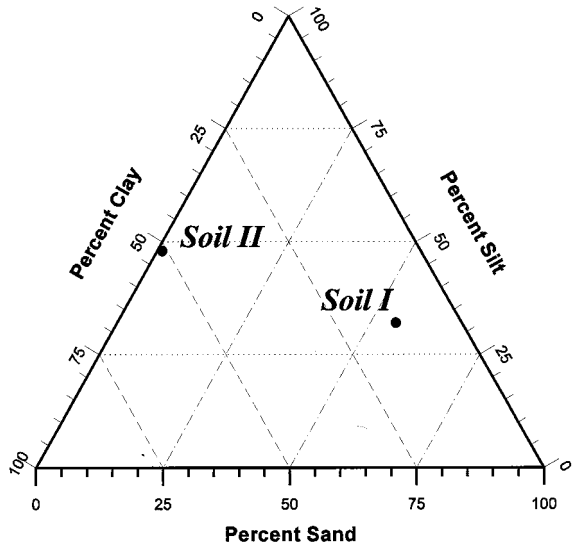

Fig. 17. Soil mixture triangle.

where $D_\nu(k_{z\nu m}) = 0$, $k_{1\nu m}^2 = \omega^2\mu_o\epsilon_1 - k_{z\nu m}^2$ and the prime indicates differentiation of D_ν with respect to the argument. The index m runs over all poles for a fixed value of ν.

The branch-cut integral in (28) is typically referred to as a continuous spectrum of modes, and it is characteristic of open-region problems [37]. Physically, it represents propagation outside the guide ($\rho > a$). The sum over m represents the discrete modes which are the main subject of this paper. For a waveguide with perfectly conducting walls, the branch-cut integral disappears and the sum over m includes an infinite number of modes. For that case, there is a finite number of poles on the real k_z axis for $|k_z| < \omega\sqrt{\mu_o\epsilon_o}$ (propagating modes) and an infinite number of poles on the imaginary k_z axis (evanescent modes). For our case with lossy walls, all of the modes have some attenuation and there is not such a clear distinction between propagating and evanescent modes. In the w-plane analysis of the previous

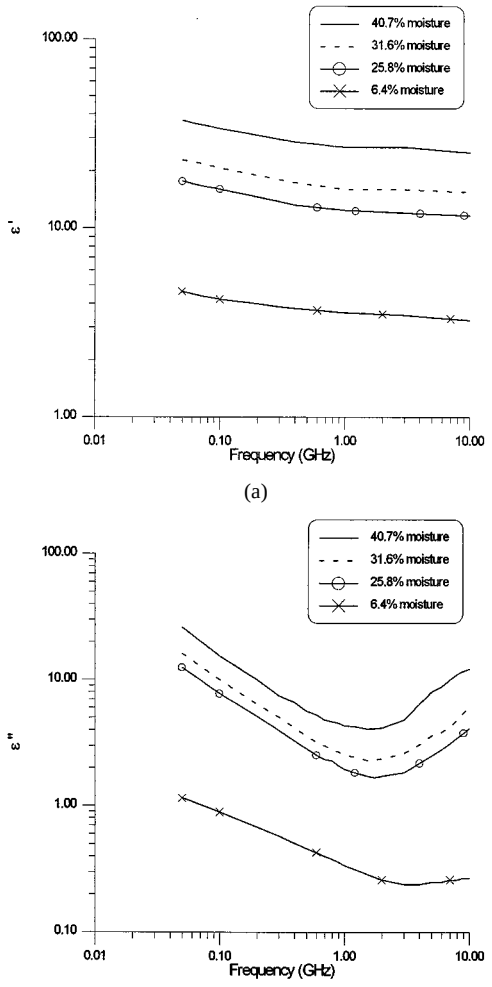

Fig. 18. Permittivity of Soil I. (a) ϵ'. (b) ϵ''.

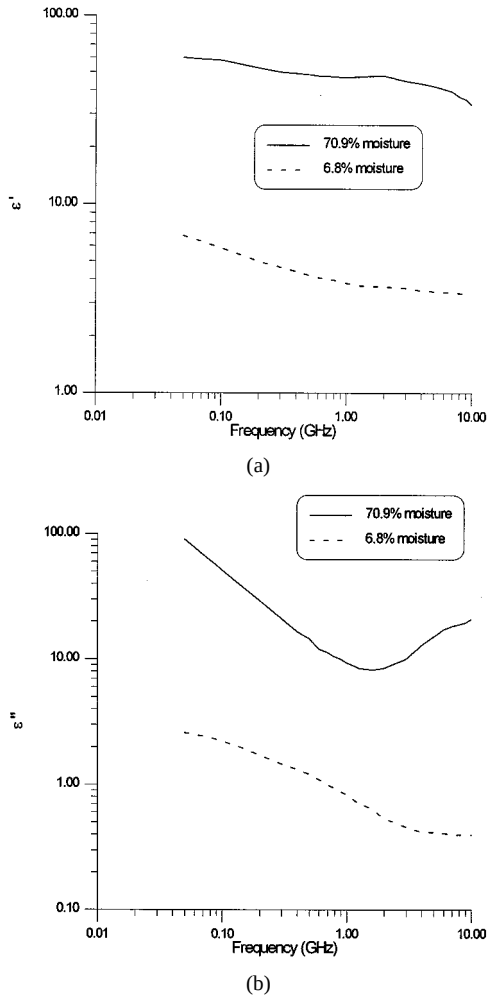

Fig. 19. Permittivity of Soil II. (a) ϵ'. (b) ϵ''.

section, we saw that some roots can intersect the branch cut and pass into another Riemann sheet. The same thing happens with the poles and the branch cut in the k_z-plane. In that case, the effect of the disappearing mode would show up in the branch-cut integral in (28). We show only a few poles in Fig. 16 because the actual number would depend on the waveguide parameters. For large values of z, the dominant field would be the mode of lowest attenuation. If none of the modes has an attenuation rate smaller than that of the external medium, then the waveguide is not very effective and most of the energy is propagating in the external medium. We would expect this behavior at low frequencies, where the waveguide radius is electrically small. In this case, the dominant field contribution might well come from the branch-cut integral.

VI. Conclusion

This paper presented the propagation characteristics of various modes of a lossy circular waveguide consisting of a soil wall with frequency-dependent electrical properties. This structure was used to simulate a wireless communications channel through tunnels, mine shafts, and boreholes. Results for different soil types and moisture levels were presented. The behavior of the attenuation as a function of moisture level, frequency, and waveguide radius is complicated. For example, it was shown that as the moisture level of the soil increases, the attenuation increases for frequencies above 100 MHz for the TM_{0m} and HE_{11} modes for a 5 m waveguide. However, this type of trend does not occur until 5 GHz for a 19-cm waveguide. For the TE_{0m} mode, as the moisture level of soil increases the attenuation decreases for frequencies above 1 GHz for both radii. In general, however, regardless of the mode type and moisture level as the frequency increases the attenuation decreases and, as a result, the attenuation of radio waves through tunnels, mine shafts, and boreholes will decrease. It was shown that for small $|k_2 a|$ some modes in the waveguide disappear, and a discussion of this behavior and how it relates to excitation problems was given. Finally, transverse field distributions for the various modes were depicted.

Radio performance predictions for underground tunnels and similar environments, that are essentially lossy waveguides, are important due to the increased reliance upon radio communications for business, government, and personal use. Perhaps the most important parameter for predicting radio performance is the signal-to-noise ratio, which depends directly on the attenuation of the propagation channel. The methodology and results presented in this paper can be used to estimate the signal-to-noise ratio based on the electrical properties of materials that

compose the walls of the lossy wave guide. Such calculations will require a knowledge of what propagation modes can be excited. Our results show that depending on the electrical parameters of the soil, not all modes will propagate (e.g., when $|k_2 a|$ is small). Understanding the character of the propagation modes that will be excited by a particular radio system is essential for the design of an effective communication system.

A comprehensive analysis of the excitation of electromagnetic fields for this type of waveguide for various antennas will be the topic of future work. It is interesting to note that, due to the complicated nature of the root locations (occurring on different Riemann sheets) of the different modes, there may be only a finite number of modes present in the waveguide. This phenomenon will also be investigated in future work.

APPENDIX
MATERIAL PROPERTIES OF SOME SOILS

One way of characterizing soils is by their fractional content of sand, silt, and clay [31]–[33], which can be described on a soil mixture triangle as shown in Fig. 17. The soil mixture triangle shows that soil types can vary significantly and, hence, the electrical properties can be quite variable. In this study we have chosen the two different soil mixtures that are distributed along the soil mixture triangle. Soil I consists of 55% sand, 32% silt, and 13% clay, while Soil II consists of 1% sand, 48% silt, and 51% clay. The percentages listed are by weight.

Figs. 18 and 19 show the measured permittivities as a function of frequency and moisture content for the two soil types used in this study. This measured data was obtained from [33]. The moisture contents in these figures are based on the ratio of volume of water to the volume of dry soil.

ACKNOWLEDGMENT

The authors would like to thank A. G. Tijhuis, Vakgroep Elektromagnetisme, Technische Universiteit Eindhoven, Eindhoven, The Netherlands, for supplying a modified version of the winding number algorithm presented in [27].

REFERENCES

[1] J. R. Wait and D. A. Hill, "Propagation along a braided coaxial cable in a circular tunnel," *IEEE Trans. Microwave Theory Tech.*, vol. MTT-23, pp. 401–405, May 1975.

[2] ——, "Electromagnetic fields of a dipole source in a circular tunnel containing a surface wave line," *Int. J. Electron.*, vol. 42, no. 4, pp. 377–391, 1977.

[3] D. A. Hill and J. R. Wait, "Analysis of radio frequency transmission in a semicircular mine tunnel containing two axial conductors," *IEEE Trans. Commun.*, vol. COM-25, pp. 1046–1050, Sept. 1977.

[4] ——, "Electromagnetic fields of a coaxial cable with an interrupted shield located in a circular tunnel," *J. Appl. Phys.*, vol. 46, no. 10, pp. 4352–4356, 1975.

[5] S. F. Mahmoud and J. R. Wait, "Calculated channel characteristics of a braided coaxial cable in a mine tunnel," *IEEE Trans. Commun.*, vol. COM-24, pp. 82–87, Jan. 1976.

[6] J. R. Wait and D. A. Hill, "Radio frequency transmission via a trolley wire in a tunnel with a rail return," *IEEE Trans. Antennas Propagat.*, vol. AP-25, pp. 248–253, Mar. 1977.

[7] R. A. Waldron, *Theory of Guided Electromagnetic Waves*. London, U.K.: Van Nostrand Reinhold, 1969, ch. 4 and 7.

[8] J. A. Stratton, *Electromagnetic Theory*. New York: McGraw-Hill, 1941, ch. 9.

[9] E. Snitzer, "Cylindrical dielectric waveguide modes," *J. Opt. Soc. Amer.*, vol. 51, no. 5, pp. 491–498, 1961.

[10] C. Yeh and G. Lindgren, "Computing the propagation characteristics of radially stratified fibers: An efficient method," *Appl. Optics*, vol. 16, no. 2, 1977.

[11] A. W. Snyder, "Asymptotic expressions for eigenfunctions and eigenvalues of a dielectric or optical waveguide," *IEEE Trans. Microwave Theory Tech.*, vol. MTT-17, pp. 1130–1138, Dec. 1969.

[12] Y. Yamaguchi and T. Sekiguchi, "Propagation characteristics of normal modes in hollow circular cylinder surrounded by dissipative medium" (in Japanese), *Trans. IECE Japan*, vol. J-62, no. 4, pp. 368–373, 1979.

[13] J. I. Glaser, "Attenuation and guidance of modes on hollow dielectric waveguides," *IEEE Trans. Microwave Theory Tech.*, vol. MTT-17, pp. 173–174, Mar. 1969.

[14] T. Abe and Y. Yamaguchi, "Propagation constant below cutoff frequency in a circular waveguide with conducting medium," *IEEE Trans. Microwave Theory Tech.*, vol. MTT-29, pp. 707–712, July 1981.

[15] C. S. Lee, S.-W. Lee, and S.-L. Chuang, "Normal modes in an overmoded circular waveguide coated with lossy material," *IEEE Trans. Microwave Theory Tech.*, vol. MTT-34, pp. 773–785, July 1986.

[16] E. A. J. Marcatili and R. A. Schmeltzer, "Hollow metallic and dielectric wave-guides for long distance optical transmission and lasers," *Bell Syst. Tech. J.*, pp. 1783–1809, July 1964.

[17] J. Brown, "Corrections to the attenuation constants of piston attenuations," *Proc. Inst. Elect. Eng.*, pt. 3, pp. 491–495, 1949.

[18] C. Dragone, "Attenuation and radiation characteristics of the $HE_1$1-mode," *IEEE Trans. Microwave Theory Tech.*, vol. MTT-28, pp. 704–710, July 1980.

[19] N. S. Kapany and J. J. Burke, *Optical Waveguides*. New York: Academic, 1972.

[20] G. Biernson and D. J. Kinsley, "Generalized plots of mode patterns in a cylindrical dielectric waveguide applied to retinal cones," *IEEE Trans. Microwave Theory Tech.*, vol. MTT-13, pp. 345–356, May 1965.

[21] P. J. B. Clarricoats, "Propagation along unbounded and bounded dielectric rods: Part 2—Propagation along a dielectric rod," *Proc. Inst. Elect. Eng.*, pt. c, pp. 177–186, Oct. 1960.

[22] A. W. Snyder, "Excitation and scattering of modes on a dielectric or optical fiber," *IEEE Trans. Microwave Theory Tech.*, vol. MTT-17, pp. 1138–1144, Dec. 1969.

[23] J. C. Chiba, T. Inaba, Y. Kuwamoto, O. Banno, and R. Sato, "Radio communication in tunnels," *IEEE Trans. Microwave Theory Tech.*, vol. MTT-26, pp. 439–443, June 1978.

[24] M. Y. Antimirov, A. A. Kolyshkin, and R. Vaillancourt, *Complex Variables*. New York: Academic, 1998.

[25] M. J. Ablowitz and A. S. Fokas, *Complex Variables: Introduction and Application*. New York: Cambridge Univ. Press, 1997.

[26] B. K. Singaraju, D. V. Giri, and C. E. Baum, "Further developments in the application of contour integration to the evaluation of the zeros of analytic functions and relevant computer programs," Air Force Weapons Lab., Mathematics Note 42, Mar. 1976.

[27] A. G. Tijhuis and R. M. van der Weiden, "SEM approach to transient scattering by a lossy, radially inhomogeneous dielectric circular cylinder," *Wave Motion*, vol. 8, pp. 43–63, 1986.

[28] E. F. Kuester, D. C. Chang, and S. W. Plate, "Electromagnetic wave propagation along horizontal wire systems in or near a layered earth," *Electromagn.*, vol. 1, no. 1, pp. 243–265, 1981.

[29] S. W. Plate, D. C. Chang, and E. F. Kuester, "Propagation modes on a buried leaky coaxial cable," Electromagn. Lab., Dept. Elect. Engrg., Univ. Colorado, Boulder, CO, Scientific Rep. 32, Mar. 1978.

[30] R. T. Ling, J. D. Scholler, and P. Y. Ufimtsev, "The propagation and excitation of surface waves in an absorbing layer," in *Progress in Electromagnetic Research, PIER 19*, J. A. Kong, Ed. Cambridge, MA: EMW, 1998, pp. 49–91.

[31] M. T. Hallikainen, F. T. Ulaby, M. C. Dobson, M. A. El-Rayes, and L.-K. Wu, "Microwave dielectric behavior of wet soil—Part I: Empirical models and experimental observation," *IEEE Trans. Geosci. Remote Sensing*, vol. GRS-23, pp. 25–34, Jan. 1985.

[32] M. C. Dobson, F. T. Ulaby, M. T. Hallikainen, and M. A. El-Rayes, "Microwave dielectric behavior of wet soil-Part II: Dielectric mixing models," *IEEE Trans. Geosci. Remote Sensing*, vol. GRS-23, pp. 35–46, Jan. 1985.

[33] J. O. Curtis, C. A. Weiss Jr., and J. B. Everett, "Effect of soil composition on complex dielectric properties," U.S. Army Corps Eng. Res., U.S. Army Eng. Waterways Experiment Station, Vicksburg, MS, Tech. Rep. EL-95-34, Dec. 1995.

[34] D. A. Hill and J. R. Wait, "Calculated transmission loss for a leaky feeder communication system in a circular tunnel," *Radio Sci.*, vol. 11, no. 4, pp. 315–321, 1976.
[35] J. R. Wait and D. A. Hill, "Impedance of an electric dipole located in a cylindrical cavity in a dissipative medium," *Appl. Phys.*, vol. 11, pp. 351–356, 1976.
[36] M. Abramowitz and I. A. Stegun, *Handbook of Mathematical Functions*. Washington, DC: Nat. Bureau Standards, 1964.
[37] J. R. Wait and D. A. Hill, "Theory of transmission of electromagnetic waves along a drill rod in conducting rock," *IEEE Trans. Geosci. Electron.*, vol. GE-17, pp. 21–24, Apr. 1979.

Christopher L. Holloway (S'86–M'92) was born in Chattanooga, TN, on March 26, 1962. He received the B.S. degree from the University of Tennessee at Chattanooga in 1986, and the M.S. and Ph.D. degrees from the University of Colorado at Boulder, in 1988 and 1992, respectively, both in electrical engineering.

During 1992, he was a Research Scientist with ElectroMagnetic Applications, Inc., in Lakewood, CO. His responsibilities included theoretical analysis and finite-difference time-domain modeling of various electromagnetic problems. From the fall of 1992 to 1994, he was with the National Center for Atmospheric Research (NCAR), Boulder, CO. While at NCAR his duties included wave propagation modeling, signal processing studies, and radar systems design. From 1994 to 2000, he was with the Institute for Telecommunication Sciences (ITS), U.S. Department of Commerce, Boulder, CO, where he was involved in wave propagation studies. Since 2000, he has been with the National Institute of Standards and Technology (NIST), Boulder, CO, where he works on electromagnetic theory. He is also on the Graduate Faculty at the University of Colorado at Boulder.

Dr. Holloway received the 1999 Department of Commerce Silver Medal for his work in electromangetic theory and the 1998 Department of Commerce Bronze Medal for his work on printed curious boards. His research interests include electromagnetic field theory, wave propagation, guided wave structures, remote sensing, numerical methods, and electromagnetic compatibility and electromagnetic interference issues. He is a member of Commission A of the International Union of Radio Science and is an Associate Editor on propagation for the IEEE TRANSACTIONS ON ELECTROMAGNETIC COMPATIBILITY.

David A. Hill (M'72–SM'76–F'87) was born in Cleveland, OH, on April 21, 1942. He received the B.S.E.E. and M.S.E.E. degrees from The Ohio University, Athens, in 1964 and 1966, respectively, and the Ph.D. degree in electrical engineering from The Ohio State University, Columbus, in 1970.

From 1970 to 1971, he was a Visiting Fellow with the Cooperative Institute for Research in Environmental Sciences, Boulder, CO, where he worked on pulse propagation. From 1971 to 1982, he was with the Institute for Telecommunications Sciences, Boulder, CO, where he worked on antennas and propagation. Since 1982, he has been with the National Institute of Standards and Technology, Boulder, CO, where he works on electromagnetic theory. He is also a Professor Adjoint in the Department of Electrical and Computer Engineering, University of Colorado, Boulder.

Dr. Hill is a member of URSI Commissions A, B, E, and F. He has served as a technical editor for the IEEE TRANSACTIONS ON GEOSCIENCE AND REMOTE SENSING and the IEEE TRANSACTIONS ON ANTENNAS AND PROPAGATION.

Roger A. Dalke received the B.S. degree in physics from the University of Colorado, Boulder, in 1971, and the M.S. and Ph.D. degrees from the Colorado School of Mines, Golden, in 1983 and 1986, respectively.

As a Research Engineer, he has developed numerical techniques for a variety of electromagnetic scattering problems as well as signal processing and imaging methods used in exploration geophysics. More recently, he has been involved in the development of computer simulation models for digital radio systems, noise and interference measurements and analysis, and radio propagation in urban environments.

George A. Hufford (S'45–M'55–LF'95) was born in San Francisco, CA, in 1927. He received the B.S. degree in engineering from the California Institute of Technology, Pasadena, in 1946, the M.S. degree in electrical engineering from the University of Washington, Seattle, in 1948, and the Ph.D. degree in mathematics from Princeton University, Princeton, NJ, in 1953.

In 1964, he joined the U.S. Department of Commerce as a member of the Tropospheric Telecommunications Laboratory, CRPL, Boulder, CO, and has remained there. The organization has undergone several name changes and is now the Telecommunications Theory Division of Institute for Telecommunication Sciences, National Telecommunication and Information Administration, in the Department of Commerce. Currently, he has been active in research related to the computation and modeling of tropospheric radio propagation under real-world conditions as when irregular terrain and a changing atmosphere are involved.

Dr. Hufford is a member of the American Mathematical Society, the Society of Industrial and Applied Mathematics, and Sigma Xi.